Fabrication and Characterization of Plasmonic Au Nanoparticles on ITO-Coated Glass Sheets

Anuradha Verma[1] · Sakshi Saxena[1,2] · Neeraj Kumar Biswas[1,3] · Anupam Srivastav[1] · Udai Bhan Singh[4] · Saif. A. Khan[5] · Rohit Shrivastav[1] · Devesh Kumar Avasthi[6] · Sahab Dass[1]

Abstract

We report here the fabrication of sputter-deposited Au nanoparticles on ITO (Sn-doped indium oxide)-coated glass substrate. The effect of varying annealing parameters, viz., time and temperature in conjunction with varying thickness parameters has been thoroughly investigated. Synthesized Au nanoparticles were characterized using a field emission scanning electron microscope (FE-SEM), Rutherford backscattering (RBS) measurement, X-ray diffraction (XRD), and optical absorbance spectroscopy. The role of annealing temperature and time duration on the evolution of Au nanoparticles has been discussed in detail based on optical absorbance spectroscopy. The present study shows that 5 nm thickness Au thin film which was annealed at 500 °C for 90 min exhibited the strongest surface plasmon resonance (SPR) effect.

Keywords Au nanoparticles · ITO · Sputtering · Annealing · Plasmons

Introduction

Plasmonic metal nanoparticles of noble metals such as Au, Ag, and Cu are of great interest because of their unique optical, electrical, and subsequent application in chemical sensors, biosensors, photonic devices, resistive random access memory (RRAM) and DNA engineering, etc., due to their unique property of surface plasmon resonance (SPR). However, the SPR properties of these nanoparticles depend upon their size and shape as well as the dielectric constant of the medium [1]. Altering the shape and size of nanostructures in the form of nanorings, nanorods, and nanospheres is quite tricky to get desired SPR properties and requires the use of various chemical and physical methods [2]. The effect of the annealing process on the evolution of Au nanorings at the surface of indium tin oxide (ITO) was reported by Ruffino et al. [3]. The size of nanoparticles and their distribution depends upon the environment in which they are grown. A recent report by Meischein et al. shows the effect on the size distribution of Ag, Au, and Cu in different ionic liquids [4]. On a similar note, the role of viscosity of ionic liquids surface in controlling the size of Au nanoparticles deposited by sputtering has been reported in the literature [5, 6]. In addition to this, the effect of annealing temperature and the atmosphere was investigated by M. Bechelany and they observed the transformation of the honeycomb mask of Au nanoparticles deposited by sputtering into the hexagonal arrays [7]. Mishra et al. investigated the effect of annealing temperature and annealing conditions on the formation of Au nanorings on the quartz substrate. In another report, a systematic investigation was made on tuning localized surface plasmon resonance (LSPR) properties of Au nanoparticles embedded in the ZnO matrix with varying temperatures from 200 to 600 °C. The redshift in LSPR was observed with increasing annealing temperature on account of the agglomeration of Au nanoparticles. The process of diffusion of

✉ Devesh Kumar Avasthi
   dka4444@gmail.com

✉ Sahab Dass
   drsahabdas@gmail.com

1   Department of Chemistry, Dayalbagh Educational Institute, Dayalbagh, Agra 282005, India

2   Institute of Applied Science, Mangalayatan University, U.P, Beswan, Aligarh-202146, India

3   Department for Continuing Education, University of Oxford, Rewley House, 1 Wellington Square, Oxford OX1 2JA, UK

4   Department of Physics, Deendayal Upadhyay Gorakhpur University, Gorakhpur 273009, India

5   Inter University Accelerator Centre, Aruna Asaf Ali Marg, New Delhi 110067, India

6   University of Petroleum and Energy Studies (UPES), Prem Nagar, Dehradun, Uttarakhand 248007, India

small Au nanocrystals during the annealing was responsible for the growth of Au nanoparticles. In another examination, the formation of silver nano cups on the surface of quartz using ultra-thin silver film and their subsequent annealing in an inert environment was also investigated by Mishra et al. The atomic force microscopy (AFM) measurements show the presence of unsymmetric islands in the as-deposited film, while annealing at 900 °C in Ar environment shows the evolution of nanocup-type structure. Ostwald ripening and buckling phenomenons were responsible for their evolution because of the existence of a metastable state during the process of annealing [8–10]. Pannu et al. demonstrated the formation of Au nanoparticles on graphene substrate by the way of varying thin film thickness which was annealed at 400 °C. The formation of Au nanoparticles with optimum thickness was responsible for engineering strain in graphene nanosheets, which in turn alters the semiconducting properties [11]. The formation of Ag nanorings was illustrated by Mohapatra et al. The nanorings are formed by the atom beam co-sputtering method through the self-assembly of Ag nanoparticles embedded in the silica matrix. The study reveals that the change in ring dimensions is due to a change in surface diffusivity of Ag nanoparticles in different substrates that is carbon and silica substrates [12]. Khan et al. adopted the glancing angle deposition method to develop aligned nanodots on a rippled silica substrate. Low energy ion beam irradiation was used to fabricate the rippled silica substrates. An atomistic simulation was performed on the annealing and deposition process by using Monte Carlo techniques to develop aligned nanodots. The study reveals that the rippled silica template/transparent substrate could be of great interest to obtain aligned metal nanoparticles with narrow size distribution for application in biosensing [13]. Singhal et al. reported the formation of Au–C_{60} nanocomposite by thermal co-evaporation followed by thermal annealing treatment from 150 to 300 °C. Evolution of broad SPR peak was observed at 250 °C and with the rise in temperature, a blue shift in SPR peak was realized due to transformation of C_{60} fullerene matrix into amorphous carbon [14]. All the reports discussed above confirm the significant role of annealing parameters and the substrate on the plasmonic properties of metal nanoparticles.

ITO (Sn-doped indium oxide)-coated glass substrates are most commonly used to prepare thin films for their application in resistive random access memory (RRAM), solar cell electrodes, photoelectrochemical water splitting studies, etc. [15–17]. The authors have prepared Au nanoparticles by various routes such as electrodeposition and citrate reduction method and examined their role in enhancing photoelectrochemical response for hydrogen generation for metal oxides viz. Fe_2O_3 and $BiVO_4/Fe_2O_3$ heterojunction, respectively [17, 18]. The motivation behind the present investigation is to get the optimum thickness, and annealing parameters to derive maximum SPR effect by adopting the sputtering method to deposit Au nanoparticles on ITO-coated glass substrates. The parameters so obtained were utilized to prepare thin films of Au/TiO_2 which were further irradiated with 500 keV Ar^{2+} ion beams for their application in PEC water splitting for hydrogen generation, and the results have been reported by the authors [19].

The present work reports the highlights of the effect of film thickness, annealing temperature, and time on the evolution of Au nanoparticles on ITO-coated glass substrate deposited by the sputtering method. Various sets of samples prepared under the present investigation are shown below in Fig. 1.

The absorbance spectrum of all 27 samples along with FE-SEM imaging was performed. The thickness of the sample was confirmed by Rutherford backscattering (RBS) measurements.

Experimental

Au thin films were deposited under inert conditions using Q150T S, Quoram Technologies, a high vacuum turbo pumped sputter coater system available at Inter-University Accelerator Center, New Delhi. Plasma in the deposition chamber was created using Ar gas under vacuum conditions and by increasing time of deposition time from 10 to 50 s to

Fig. 1 Schematic presentation of samples prepared by adopting different thicknesses and annealing parameters
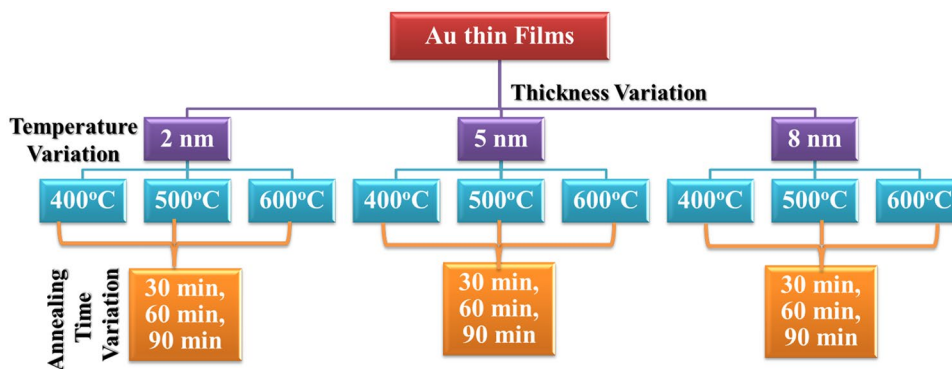
deposit three different thicknesses of 2 nm, 5 nm, and 8 nm on cleaned ITO-coated glass substrates. The as-deposited thin films were then annealed for the different time durations (30 min, 60 min, and 90 min) and at each annealing temperature, viz. 400 °C, 500 °C, and 600 °C in an inert N_2 atmosphere.

Thin films so obtained were characterized by FE-SEM instrument (MIRA II LMH from TESCAN) for surface morphology at IUAC, New Delhi. The chemical analysis of the samples was carried out using Oxford Instruments energy dispersive spectrometry (EDS) attached with the AZTEC program at a working distance of 15 mm, voltage 15 kV, and X-ray counts up to 90 s, utilizing a facility at the Department of Chemistry, DEI, Dayalbagh, Agra. The elemental peaks were resolved with the AUTOID program of the system. EDS facility is the fitment of a JEOL JSM-7610F PLUS field emission scanning electron microscope (FESEM).

The samples were also observed in XRD, which was performed with Bruker D8 AdVANCE with Cu Kα radiation source with 2θ scan range of 20–60° with a scan speed of 2 s/step and step size of 0.05°. UV–visible optical absorbance spectroscopy was performed by a double-beam UV–visible spectrometer, UV-1800, Shimadzu, Japan. XRD and optical absorbance facilities were availed at the Department of Chemistry, DEI, Dayalbagh, Agra.

The areal concentration of Au in the sample was determined by RBS experimental technique where a 2-MeV He ion beam from a 1.7-MV Pelletron accelerator was used to record the Rutherford backscattering spectrum. A silicon surface barrier detector having a resolution of 20 keV was used for finding backscattered He ions at an angle of 165° from the beam direction with a solid angle of 1 msr. The SIMNRA software, which is a Microsoft Windows program, is utilized to simulate and analyze the backscattering spectra. RBS measurements were performed using tandem accelerator facilities available at Inter University Accelerator Center, New Delhi.

Results and Discussion

Microscopic Imaging and EDS Measurements

The particle size distribution of all the samples was determined from FE-SEM images. The ImageJ software was used to get the average particle size of particles. A typical FE-SEM image of plane/pristine ITO glass substrate is given below in Fig. 2.

Figures 3, 4, and 5(a–i) show the FESEM image for various annealing time and temperature. It is shown for all three different thicknesses. The inset of FE-SEM micrographs shows the particle size distribution.
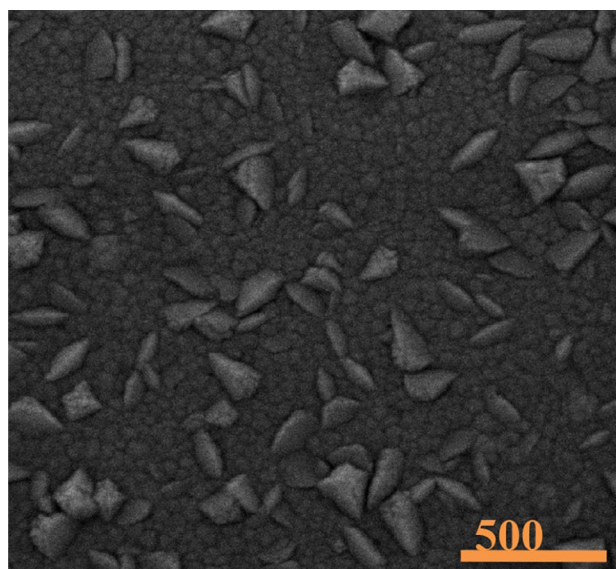

Fig. 2 FE-SEM micrograph of plane ITO substrate

In the case of a 2-nm-thick Au film, the average particle size lies in the range of 24–34 nm. From the particle size distribution shown in Fig. 6, with an increase in time and temperature for annealing, the particle size tends to increase. A similar trend of increase in particle size with a rise in temperature rise on SiO_2 substrate was reported by Kwon et al., which is showing an increasing trend [5].

As can be seen in Figs. 4 and 5, for 5- and 8-nm thicknesses at the lowest annealing temperature of 400 °C, dewetting was observed. An increase in annealing time for 5-nm-thick Au film at 500 °C led to an increase in particle size from 77 to 83 nm. At 600 °C, 78 to 94 nm increase in particle size was observed by increasing annealing time. When the duration was raised to 90 min, particle fragmentation was observed, indicating that high temperature and time for annealing are responsible for the dissolution of particles at the surface.

At the highest thickness, i.e., 8 nm taken in the present study, dewetting was observed at the lowest temperature of 400 °C. On increasing annealing temperature to 500 °C, the particle size of 171 and 170 nm was obtained at 60- and 90-min annealing time, while for 30 min annealing time average particle size was 256 nm, showing agglomeration of Au nanoparticles. On further increasing annealing temperature up to 600 °C, particle dissolution was observed showing a reduction in particle size.

EDS measurements of pure ITO glass and Au thin film of 5 nm thickness (500 °C, 90 min) and 8 nm thickness (400 °C, 30 min) were also performed as shown below in Fig. 7. Pure ITO substrate shows the peak of In, O, and Sn while the peak of Au is clearly visible in Au deposited and
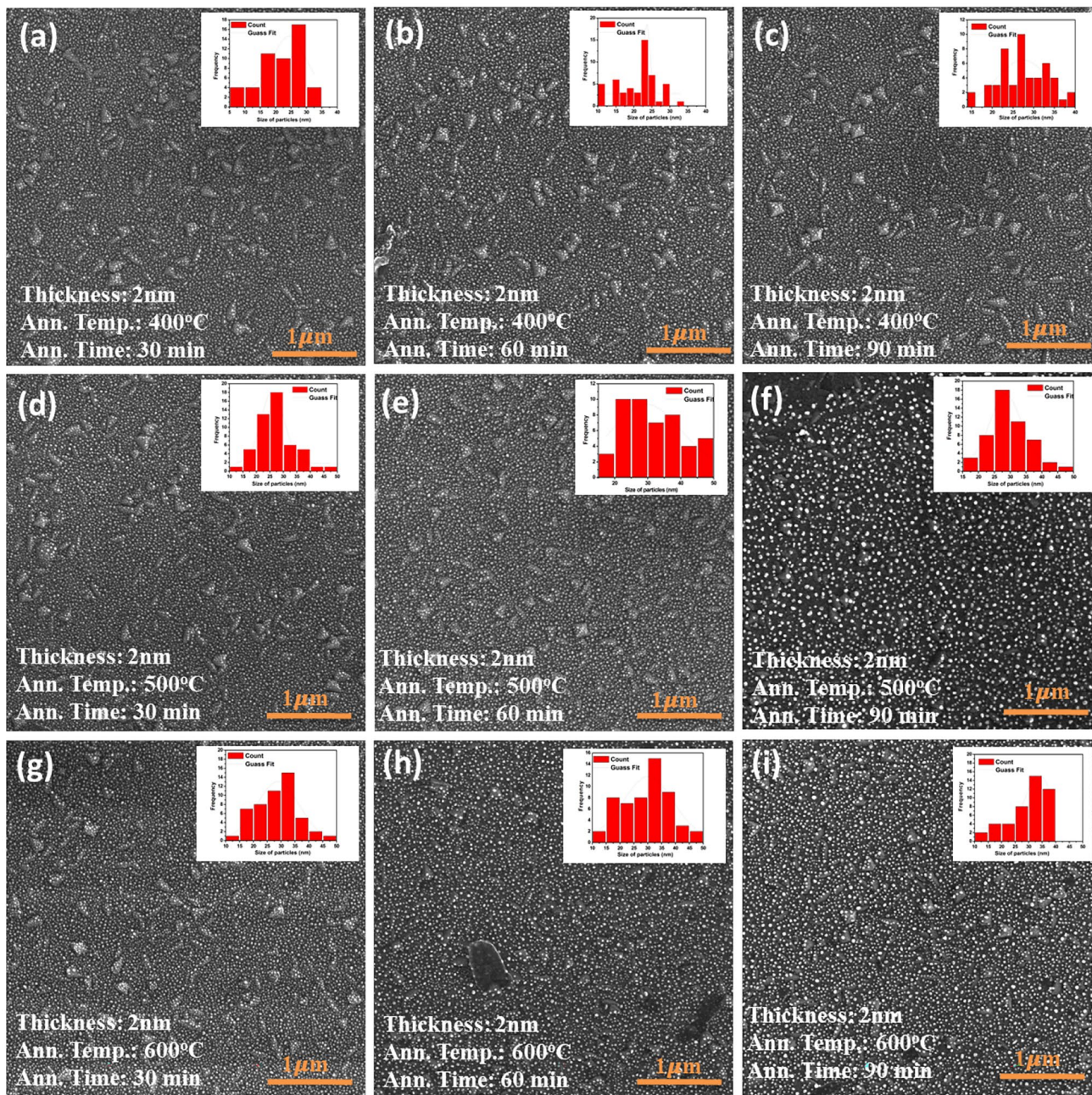
Fig. 3 (a-i) FE-SEM micrographs of 2-nm-thick Au film annealed for different time durations at varied annealing temperatures

annealed on ITO glass substrate. The EDS spectrum shows 5.4 wt% of Au in 5 nm thickness film and 9.6 wt% of Au in 8-nm-thickness film.

Optical Measurements

To confirm the effect of annealing on sputter-deposited nanoparticles, the absorbance spectra of plane ITO sheet and as-deposited films were recorded and are presented in

Fig. 8. It is clearly visible from the figure that the absorbance spectra of as-deposited Au thin films match well with the plane ITO, which confirms the absence of nanoparticle formation that was responsible for the SPR peak.

Figure 9a–c shows absorbance spectra for 2-nm-thick film. The broad absorbance is visible on account of the variable size of particles up to 500 °C. At a high temperature of 600 °C, maximum absorbance was attained at 90 min annealing time which shows direct relation with increasing particle size.
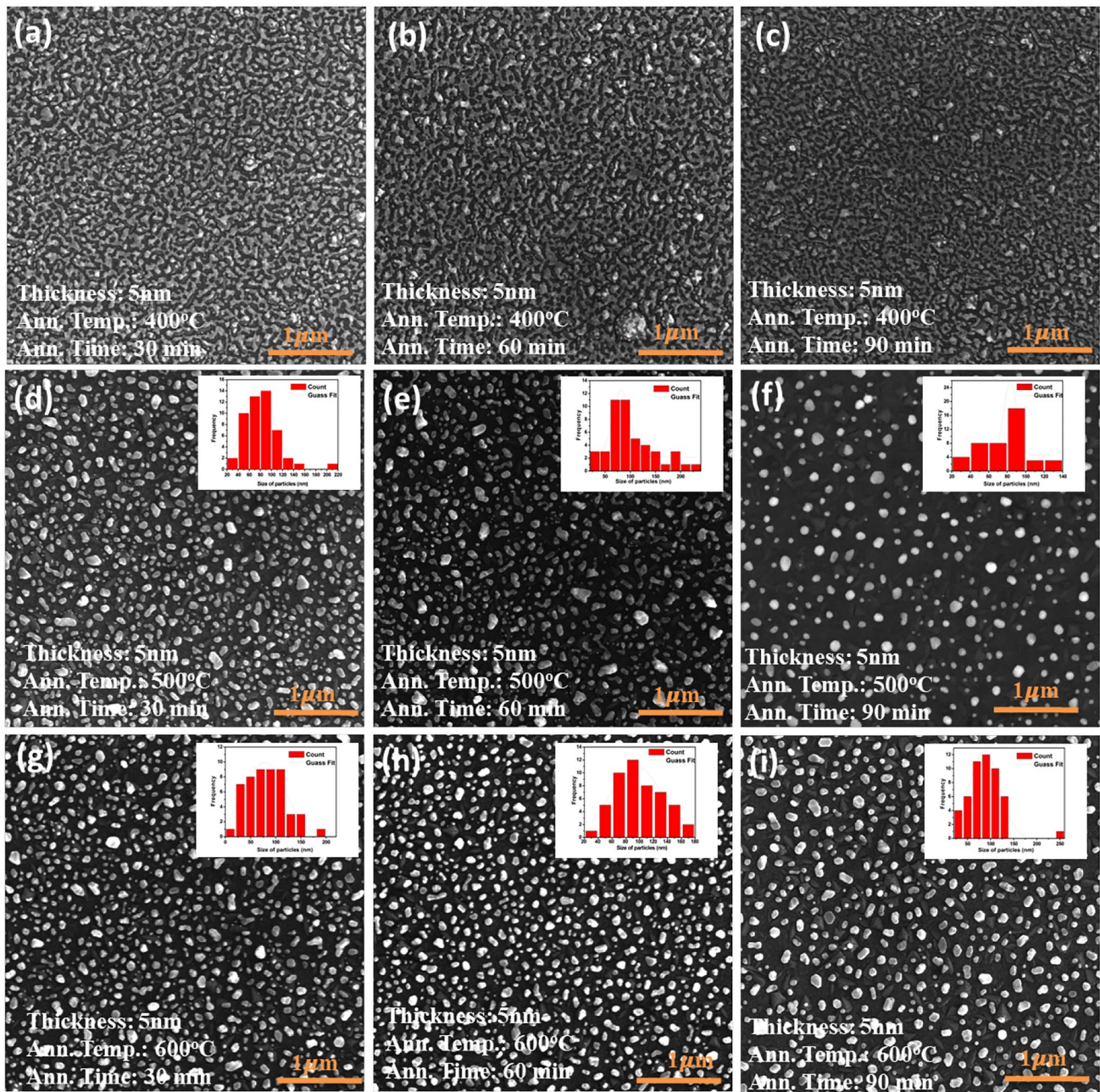
Fig. 4 (a-i) FE-SEM micrographs of 5-nm-thick Au film annealed for different time durations at varied annealing temperatures

In the case of 5-nm-thick films, absorbance at low temperature does not show SPR due to dewetting of films (Fig. 9d). At 500 and 600 °C, maximum intensity SPR peaks are visible at 90 and 60 min annealing time, respectively, and the SPR peak intensity shows direct dependency on the particle size of nanoparticles so formed (Fig. 9e, f).

Likewise for 8-nm-thick film, dewetting was prominent at a low annealing temperature of 400 °C. At high temperatures, particle size shows harmony with the calculated average particle size. The shift in SPR peak toward higher wavelength was observed due to the bigger-sized Au nanoparticles, and in addition to this, reduced absorbance is a result of prevalent light scattering by larger size Au particles.

From the UV–vis spectroscopy, it is clear that for 2- and 8-nm-thick Au thin films, no clear signature of SPR is as such visible. Thus, for 5-nm-thick Au film (annealed at 500 and
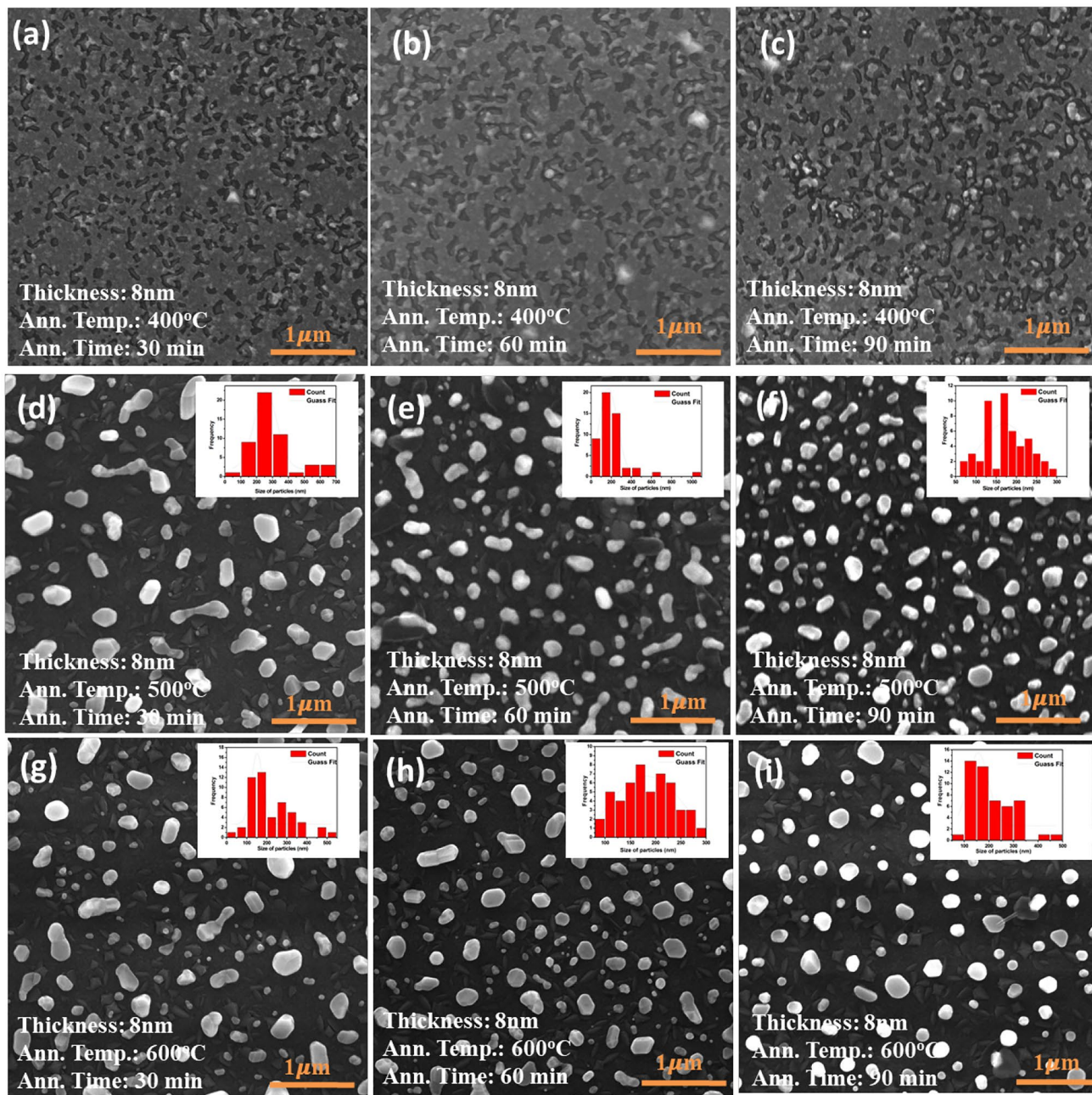
Fig. 5 (a-i) FE-SEM micrographs of 8-nm-thick Au film annealed for different time durations at varied annealing temperatures

600 °C) was taken to see the dependence of surface plasmon resonance peak position on average particle size (Fig. 10). For 5-nm-thick Au film annealed at 400 °C, film dewetting was prominent. At 500 °C, with an increase in annealing time, particle size increases, and SPR peak is shifting toward higher wavelength, i.e., redshift is visible. On increasing annealing temperature to 600 °C, the redshift in SPR peak is observed up to 60 min annealing time, but for 90 min annealing, particle size reduces from 94 (60 min annealing) to 86 nm on account of particle dissolution, which results in

a shift of SPR peak from 633 to 629 nm. This can also be inferred that high annealing temperature does not influence SPR peak position at large with increasing annealing time.

RBS Measurements

The RBS spectra of three thicknesses of Au films on ITO-coated glass are shown in Fig. 11, and all RBS peaks related to Au, Sn, In, Si, and O have been assigned. The area under the RBS peak reveals the areal concentration of a particular
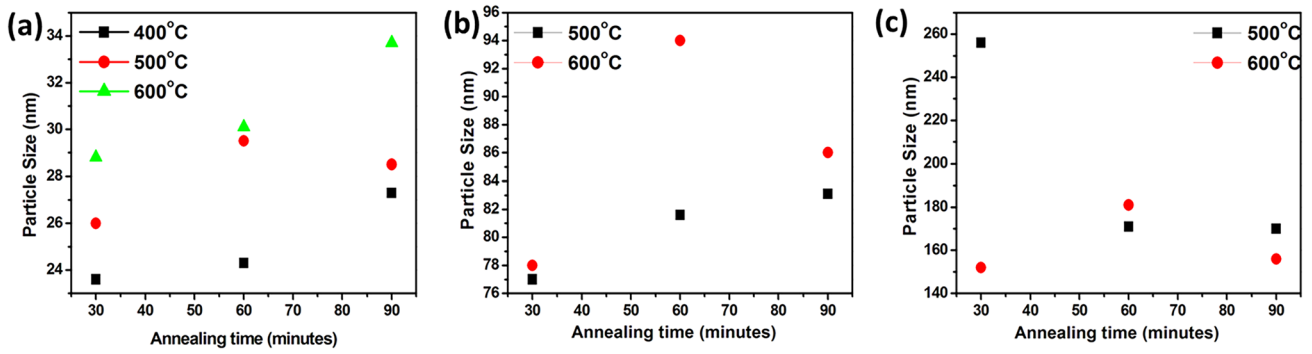
Fig. 6 Average particle size distribution of **a** 2-nm-, **b** 5-nm-, and **c** 8-nm-thick films recorded at varying annealing parameters

element. With an increase in the thickness of Au from 2 to 8 nm, the area under the Au RBS peak is increased, and this confirms that the area concentration of Au has been increased,

Fig. 7 EDS spectrum of **a** ITO substrate, **b** Au thin film of 5 nm, and **c** 8 nm thickness

as also suggested by an experiment. The areal concentration of the element is calculated using the formula given below [20]:

$$N_c = \frac{Y \sin \alpha}{N_p \frac{\partial \sigma}{\partial \Omega} \Omega}$$

where N_c is an areal concentration for Au element in the RBS spectra, N_p is the number of incidents of He ions, Ω ($=1$ msr) is the solid angle subtended by the detector, α ($=90°$) is the angle between beam direction and the sample surface, and ($\partial\sigma/\partial\Omega$) is the differential Rutherford backscattering cross-section. The areal concentration of Au on the ITO-coated glass substrate is calculated and mentioned in Table 1. The recorded spectrum is shown in Fig. 11 confirms the presence of Au at channel no. 1800.

In literature, the RBS studies reported by the Kumar et al. reveal diffusion of Ag atoms in glass as a result of post-annealing that leads to a decrease in peak height of Ag [21, 22], while in the present study, as such, no change in peak intensity can be seen as an effect of post-annealing.
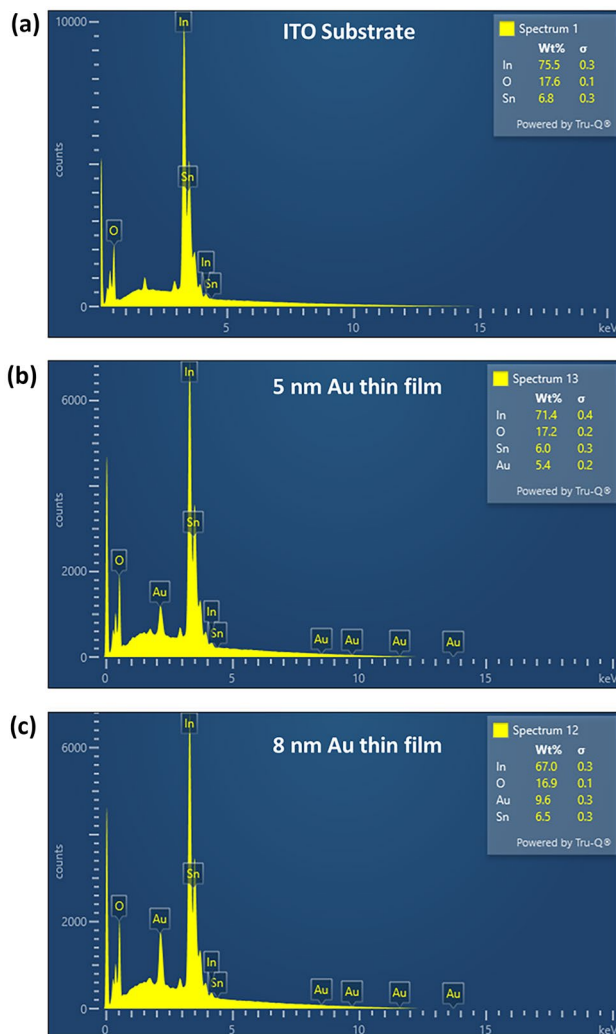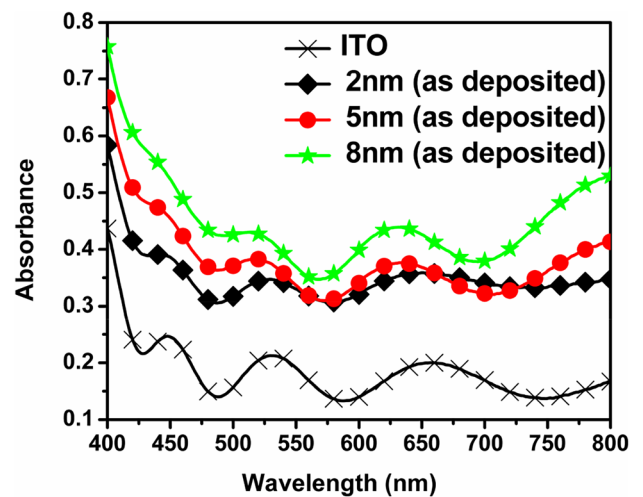

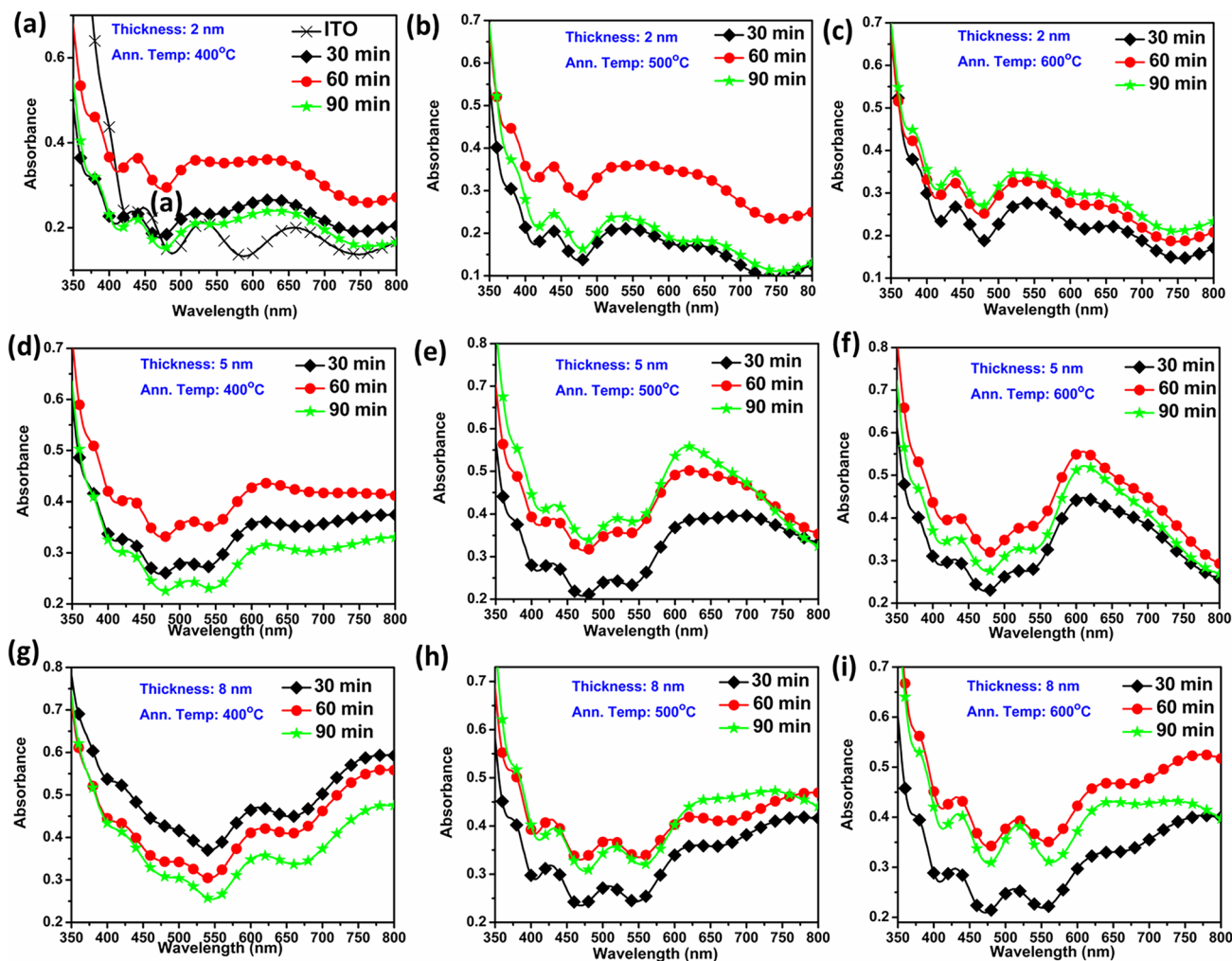**Fig. 8** Absorbance spectra of plane ITO along with as-deposited thin films

Fig. 9 Absorbance spectra of Au thin films. **a–c** 2 nm Au thin films annealed at 400 °C, 500 °C, and 600 °C for different time durations; **d–f** 5 nm Au thin films annealed at 400 °C, 500 °C, and 600 °C for different time durations; **g–i** 8 nm Au thin films annealed at 400 °C, 500 °C, and 600 °C for different time durations at varied annealing temperatures

X-ray Diffraction Studies

To study the effect of thermal treatment on Au thin films and, correspondingly, on ITO substrate, 5-nm-thick Au film was selected for XRD measurements (see Fig. 12). The selected thin films were annealed for 60-min duration at 400 °C, 500 °C, and 600 °C. The XRD patterns do not show any impurity peaks except for the peaks of Au (JCPDS card no. 04–0784) and ITO (JCPDS card no. 44–1087), which confirms that annealing at high temperatures does not affect the crystallinity of Au as well as ITO substrate. Moreover, ITO is stable up to 600 °C [23, 24]. In the case of Au, it can be seen that with a temperature rise, Au peak intensity is increasing on account of an increase in particle size. The findings match the average particle size obtained from FESEM analysis. Kumar et al. also reported an increase in peak intensity of Ag nanoparticles with an increase in annealing temperature [21].

A Mechanism for the Growth of Nanoparticles

The process of thermal annealing affects the optical properties of noble metal particles. Cu nanoparticles deposited on phosphate glass, borosilicate glass, and natural plagioclase mineral crystal have been investigated regarding the role of thermal annealing on SPR evolution in-depth in past reports by various authors [25–27]. Likewise, the effect of thermal annealing in silver nanocrystals in soda-lime glass, and Au nanoparticles in sodium zinc borate glass have been studied in detail by Kumar et al. [21, 22, 28, 29].

From the reports discussed above, this can be said that role of thermal annealing is well established in affecting the SPR properties of Cu, Ag, and Au nanoparticles. In the present study, the optical absorbance spectra of as-deposited Au thin films of 2 nm, 5 nm, and 8 nm thickness
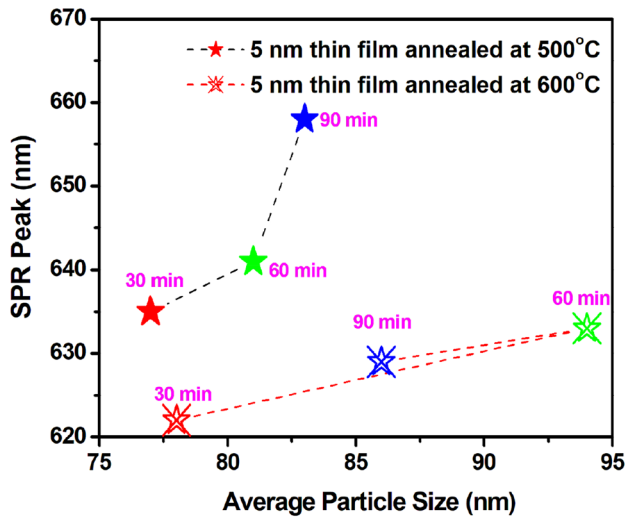
Fig. 10 SPR peak versus average particle size distribution plot for 5-nm-thick Au film annealed at 500 and 600 °C

Fig. 12 XRD plots of 5 nm Au thin film annealed for 60 min at 400 °C, 500 °C, and 600 °C

was matching with the ITO substrate except there is an increase in peak intensity with increasing thickness of Au film (see Fig. 8). During the process of thermal annealing, there starts a process of formation of nanoparticles and this is clearly visible from the evolution of SPR peaks in optical absorbance spectra provided in Fig. 9. Though for the lowest thickness of 2 nm Au film, particles of 24–34 nm
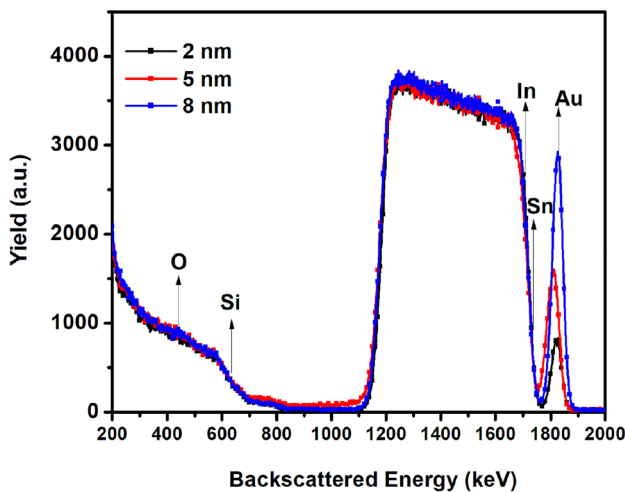
size are present. In the case of 5-nm- and 8-nm-thick Au film, initially, a low temperature of 400 °C does not facilitate nanoparticle formation even for a longer duration of annealing, and film dewetting was noticed. But, as the temperature rises to 500 °C and 600 °C, the formation of nanoparticles is visible and has been discussed in detail in the "Microscopic Imaging and EDS Measurements" and "Optical Measurements" sections. During the process of annealing, particle growth is observed by the agglomeration process up to a limited annealing duration by a process of Ostwald ripening, and then the dissolution of the particle is seen as a consequence of low binding energy of surface atoms [2, 8]. The growth of nanoparticles under thermal annealing is well described by Oswald ripening and the equations governing the process. The details of the process and equations have been well described in the literature [30]. In the current investigation, ITO substrate does affect the formation of nanoparticles, yet thermal annealing does not ensue implantation of Au nanoparticles in ITO, which has been confirmed through RBS and XRD studies.

Fig. 11 RBS spectrum of Au thin films

Table 1 Thickness of Au thin films by SIMNRA simulation

Film identity	Areal concentration	Film thickness
2 nm, 500 °C, 60 min	17×10^{15} atoms/cm^2	2.8 nm
5 nm, 500 °C, 90 min	41×10^{15} atoms/cm^2	6.9 nm
8 nm, 400 °C, 30 min	63×10^{15} atoms/cm^2	10.6 nm

Conclusion

The investigation on annealing of Au thin films with different thicknesses for different time durations revealed that 5 nm thickness annealed at 500 °C temperature for 90 min duration offers the best SPR effect. Besides this, it was also observed that dewetting of films occurs at low annealing temperature while increased temperature and annealing time leads to particle fragmentation. The study aimed to obtain suitable conditions to use these nanoparticles as visible-light sensitizers.

Author Contribution Anuradha Verma: conceptualization, methodology, writing—original draft preparation, investigation. Sakshi Saxena: data curation, editing, and formal analysis. Neeraj Kumar Biswas: visualization and data curation. Anupam Srivastav: conceptualization and visualization. Uday Bhan Singh: software and validation. Saif A Khan: visualization and data curation. Rohit Shrivastav: data curation and visualization. Devesh Kumar Avasthi: supervision, writing—reviewing and editing, conceptualization, and validation. Sahab Dass: supervision, research activity planning, writing—reviewing and editing.

Data Availability The data used to support the findings of this study are included within the article and no additional source data are required.

Declarations

Competing Interests The authors declare no competing interests.

References

1. Garcia M (2012) Surface plasmons in metallic nanoparticles: fundamentals and applications. J Phys D Appl Phys 45:389501
2. Mishra YK, Mohapatra S, Kabiraj D, Tripathi A, Pivin J, Avasthi D (2007) Growth of Au nanostructures by annealing electron beam evaporated thin films. J Opt A: Pure Appl Opt 9:S410
3. Ruffino F, Crupi I, Simone F, Grimaldi M (2011) Formation and evolution of self-organized Au nanorings on indium-tin-oxide surface. Appl Phys Lett 98:023101
4. Meischein M, Fork M, Ludwig A (2020) On the effects of diluted and mixed ionic liquids as liquid substrates for the sputter synthesis of nanoparticles. Nanomaterials 10:525
5. Kwon JY, Yoon TS, Kim KB, Min SH (2003) On the effects of diluted and mixed ionic liquids as liquid substrates for the sputter synthesis of nanoparticles. J Appl Phys 93:3270–3278
6. Vanecht E, Binnemans K, Seo JW, Stappers L, Fransaer J (2011) Growth of sputter-deposited gold nanoparticles in ionic liquids. Phys Chem Chem Phys 13:13565–13571
7. Bechelany M, Maeder X, Riesterer J, Hankache J, Lerose D, Christiansen S, Michler J, Philippe L (2010) Synthesis mechanisms of organized gold nanoparticles: influence of annealing temperature and atmosphere. Cryst Growth Des 10:587–596
8. Mishra YK, Kabiraj D, Sulania I, Pivin JC, Avasthi DK (2007) Synthesis and characterization of gold nanorings. J Nanosci Nanotechnol 7(6):1878–1881
9. Mishra YK, Adelung R, Kumar G, Elbahri M, Mohapatra S, Singhal R, Tripathi A, Avasthi DK (2013) Formation of self-organized silver nanocup-type structures and their plasmonic absorption. Plasmonics 8(2):811–815
10. Mishra YK, Mohapatra S, Singhal R, Avasthi DK, Agarwal DC, Ogale SB (2008) Au–ZnO: a tunable localized surface plasmonic nanocomposite. Appl Phys Lett 92(4):043107
11. Pannu C, Singh UB, Kumar S, Tripathi A, Kabiraj D, Avasthi DK (2014) Engineering the strain in graphene layers with Au decoration. Appl Surf Sci 308:193–198
12. Mohapatra S, Mishra YK, Tripathi A, Kabiraj D, Avasthi DK (2011) Synthesis of silver nanorings by atom beam sputtering. Int J Nanomanuf 7(1):21–29
13. Khan SA, Avasthi DK, Agarwal DC, Singh UB, Kabiraj D (2011) Quasi-aligned gold nanodots on a nanorippled silica surface: experimental and atomistic simulation investigations. Nanotechnology 22(23):235305
14. Singhal R, Sharma P, Vishnoi R, Avasthi DK (2017) Synthesis and characterizations of Au-C_{60} nanocomposite. J Alloy Compd 696:9–15
15. Tsai T, Chang K, Chang T, Zhang R et al (2016) High-performance ultraviolet 385-nm GaN-Based LEDs with embedded nanoscale air voids produced through atomic layer deposition and Al_2O_3 Passivation. IEEE Electron Device Lett 37(4)
16. Lucarelli G, Brown TM (2019) Development of highly bendable transparent window electrodes based on MoOx, SnO2, and Au dielectric/metal/dielectric stacks: application to indium tin Oxide (ITO)-free perovskite solar cells. Front Mater 6(310)
17. Verma A, Srivastav A, Banerjee A, Sharma D, Sharma S, Singh UB, Satsangi VR, Shrivastav R, Avasthi DK, Dass S (2016) Plasmonic layer enhanced photoelectrochemical response of Fe_2O_3 photoanodes. J Power Sources 315:152–160
18. Verma A, Srivastav A, Khan SA, Satsangi VR, Shrivastav R, Avasthi DK, Dass S (2017) Enhanced photoelectrochemical response of plasmonic Au embedded $BiVO_4$/Fe_2O_3 heterojunction. Phys Chem Chem Phys 19(23):15039–15049
19. Verma A, Srivastav A, Sharma D, Banerjee A, Sharma S, Satsangi VR, Shrivastav R, Avasthi DK, Dass S (2016) A study on the effect of low energy ion beam irradiation on Au/TiO_2 system for its application in photoelectrochemical splitting of water. Nucl Instrum Methods Phys Res Sect B 379:255–261
20. Singh UB, Pannu C, Agarwal DC, Ojha S, Khan SA, Ghosh S, Avasthi DK (2017) Large electronic sputtering yield of nanodimensional Au thin films: dominant role of thermal conductivity and electron phonon coupling factor. J Appl Phys 121(9):095308
21. Kumar P, Mathpal MC, Prakash J, Hamad S, Rao SV, Viljoen BC, Duvenhage MM, Njoroge EG, Roos WD, Swart HC (2019) Study of tunable plasmonic, photoluminscence, and nonlinear optical behavior of Ag nanoclusters embedded in a glass matrix for multifunctional applications. Phys Status Solidi A 216(4):1800768
22. Kumar P, Mathpal MC, Tripathi AK, Prakash J, Agarwal A, Ahmad MM, Swart HC (2015) Plasmonic resonance of Ag nanoclusters diffused in soda-lime glasses. Phys Chem Chem Phys 17(14):8596–8603
23. Premkumar M, Vadivel S (2017) Effect of annealing temperature on structural, optical and humidity sensing properties of indium tin oxide (ITO) thin films. J Mater Sci: Mater Electron 28(12):8460–8466
24. Khusayfan NM, El-Nahass MM (2013) Study of structure and electro-optical characteristics of indium tin oxide thin films. Adv Condens Matter Phys
25. Zhou Q, Wang C, Shen AH (2021) Copper nanoparticles embedded in natural plagioclase mineral crystals: in situ formation and third-order nonlinearity. J Phys Chem C 126(1):387–395
26. Jiménez JA (2019) Thermal effects on the surface plasmon resonance of Cu nanoparticles in phosphate glass: impact on Cu+ luminescence. Nanoscale Advances 1(5):1826–1832
27. Xiang W, Gao H, Ma L, Ma X, Huang Y, Pei L, Liang X (2015) Valence state control and third-order nonlinear optical properties of copper embedded in sodium borosilicate glass. ACS Appl Mater Interfaces 7(19):10162–10168
28. Kumar P, Mathpal MC, Ghosh S, Inwati GK, Maze JR, Duvenhage MM, Roos WD, Swart HC (2022) Plasmonic Au nanoparticles embedded in glass: study of TOF-SIMS, XPS and its enhanced antimicrobial activities. J Alloy Compd 909:164789
29. Kumar P, Mathpal MC, Jagannath G, Prakash J, Maze JR, Roos WD, Swart HC (2021) Optical limiting applications of resonating

plasmonic Au nanoparticles in a dielectric glass medium. Nanotechnology 32(34):345709

30. Westen TV, Groot RD (2018) Effect of temperature cycling on ostwald ripening. Cryst Growth Des 18(9):4952–4962

Publisher's Note Springer Nature remains neutral with regard to jurisdictional claims in published maps and institutional affiliations.